Research Article

LTE Adaptation for Mobile Broadband Satellite Networks

Francesco Bastia, Cecilia Bersani, Enzo Alberto Candreva, Stefano Cioni, Giovanni Emanuele Corazza, Massimo Neri, Claudio Palestini, Marco Papaleo, Stefano Rosati, and Alessandro Vanelli-Coralli

ARCES, University of Bologna, Via V. Toffano, 2/2, 40125 Bologna, Italy

Correspondence should be addressed to Stefano Cioni, scioni@arces.unibo.it

One of the key factors for the successful deployment of mobile satellite systems in 4G networks is the maximization of the technology commonalities with the terrestrial systems. An effective way of achieving this objective consists in considering the terrestrial radio interface as the baseline for the satellite radio interface. Since the 3GPP Long Term Evolution (LTE) standard will be one of the main players in the 4G scenario, along with other emerging technologies, such as mobile WiMAX; this paper analyzes the possible applicability of the 3GPP LTE interface to satellite transmission, presenting several enabling techniques for this adaptation. In particular, we propose the introduction of an inter-TTI interleaving technique that exploits the existing H-ARQ facilities provided by the LTE physical layer, the use of PAPR reduction techniques to increase the resilience of the OFDM waveform to non linear distortion, and the design of the sequences for Random Access, taking into account the requirements deriving from the large round trip times. The outcomes of this analysis show that, with the required proposed enablers, it is possible to reuse the existing terrestrial air interface to transmit over the satellite link.

1. Introduction and Motivation

Integrated terrestrial and satellite communication system is a paradigm that has been addressed for many years and that is at the fore front of the research and development activity within the satellite community. The recent development of the DVB-SH standard [1] for mobile broadcasting demonstrates that virtuous synergies can be introduced when terrestrial networks are complemented with a satellite component able to extend their service and coverage capabilities. A key aspect for the successful integration of the satellite and terrestrial components is the maximization of technological commonalities aimed at the exploitation of the economy of scale that derives from the vast market basis achievable by the integrated system. In order to replicate in 4G networks the success of the integrated mobile broadcasting systems, many initiatives are being carried out [2, 3] for the design of a satellite air interface that maximizes the commonalities with the 4G terrestrial air interface. These initiatives aim at introducing only those modifications that are strictly

needed to deal with the satellite channel peculiarities, such, for example, nonlinear distortion introduced by the on-board power amplifiers, long round-trip propagation times, and reduced time diversity, while keeping everything else untouched. Specifically, it is important to highlight the different mobile channel propagation models between terrestrial and satellite environments. In fact, in terrestrial deployments, channel fades are typically both time and frequency selective, and are counteracted by the use of opportunistic scheduling solutions, which select for each user the time slots and the frequency bands where good channel conditions are experienced. On the other hand, satellite links are characterized by large round trip delay, which hinders the timeliness of the channel quality indicators and sounding signals, continuously exchanged between users and terrestrial base stations. Further, satellite channel fades are typically frequency-flat, due to the almost Line-of-Sight (LOS) nature of propagation in open area environments, thus alternative solutions have to be designed in order to increase the satellite link reliability.

In this framework, this paper investigates the adaptability of the 3GPP Long Term Evolution (LTE) standard [4] to the satellite scenarios. The 3GPP LTE standard is in fact gaining momentum and it is easily predictable to be one of the main players in the 4G scenario, along with other emerging technologies such as mobile WiMAX [5]. Thanks to this analysis, we propose the introduction of few technology enablers that allow the LTE air interface to be used on a satellite channel. In particular, we propose the following:

(i) an inter-TTI (Transmission Time Interval) interleaving technique that is able to break the channel correlation in slowly varying channels by exploiting the existing H-ARQ facilities provided by the LTE physical layer;

(ii) the introduction of PAPR reduction techniques to increase the resilience of the OFDM waveform to nonlinear distortions;

(iii) a specific design of the sequences for the random access scheme, taking into account the requirements deriving from large satellite round trip times.

In addition, with the aim of further enhancing the robustness to long channel fades, an Upper-Layer (UL) Forward Error Correction (FEC) technique is also proposed and compared with the inter-TTI technique.

According to market and business analysis [6], two application scenarios are considered: mobile broadcasting using linguistic beams with national coverage and two-way communications using multispot coverage with frequency reuse. Clearly, the service typologies paired with these two application scenarios have different requirements in terms of data rates, tolerable latency, and QoS. This has been taken into account into the air interface analysis.

2. GPP LTE: Main Features

The 3GPP LTE air interface is shortly summarized to ensure self-containment and to provide the perspective for the introduction of advanced solutions for the adaptation to satellite links, as described in Section 3.

The FEC technique adopted by LTE for processing the information data is a Turbo scheme using Parallel Concatenated Convolutional Code (PCCC) [7]. Two 8-state constituent encoders are foreseen and the resulting coding rate is 1/3. The LTE technical specifications provide several values for the input block size K_{TC} to the Turbo encoder, varying form $K_{TC} = 40$ up to $K_{TC} = 6144$. After channel encoding, the Circular Buffer (CB) and Rate Matching (RM) block allows to interleave, collect and select the three input streams coming from the Turbo encoder (systematic bits, parity sequence from encoder-1 and encoder-2), as depicted in Figure 1. The three input streams are processed with the following steps.

(1) Each of the three streams is interleaved separately by a sub-block interleaver.

(2) The interleaved systematic bits are written into the buffer in sequence, with the first bit of the interleaved systematic bit stream at the beginning of the buffer.

(3) The interleaved P1 and P2 streams are interlaced bit by bit. The interleaved and interlaced parity bit streams are written into the buffer in sequence, with the first bit of the stream next to the last bit of the interleaved systematic bit stream.

(4) Eight different Redundancy Versions (RVs) are defined, each of which specifies a starting bit index in the buffer. The transmitter reads a block of coded bits from the buffer, starting from the bit index specified by a chosen RV. For a desired code rate of operation, the number of coded bits N_{data} to be selected for transmission is calculated and passed to the RM block as an input. If the end of the buffer is reached and more coded bits are needed for transmission, the transmitter wraps around and continues at the beginning of the buffer, hence the term of "circular buffer." Therefore, puncturing, and repetition can be achieved using a single method.

The CB has an advantage in flexibility (in code rates achieved) and also granularity (in stream sizes). In LTE, the encoded and interleaved bits after the RM block are mapped into OFDM symbols. The time unit for arranging the rate matched bits is the Transmission Time Interval (TTI).

Throughout all LTE specifications, the size of various fields in the time domain is expressed as a number of time units, $T_s = 1/(15000 \times 2048)$ seconds. Both downlink and uplink transmissions are organized into radio frames with duration $T_f = 307200T_s = 10$ ms. In the following, the *Type-1* frame structure, applicable to both FDD and TDD interface, is considered. Each radio frame consists of 20 slots of length $T_{slot} = 15360T_s = 0.5$ ms, numbered from 0 to 19. A sub-frame is defined as two consecutive slots, where sub-frame i consists of slots $2i$ and $2i + 1$. A TTI corresponds to one sub-frame.

In general, the baseband signal representing a downlink physical channel is built through the following steps:

(i) scrambling of coded bits in each of the code words to be transmitted on a physical channel;

(ii) modulation of scrambled bits to generate complex-valued modulation symbols;

(iii) mapping of the complex-valued modulation symbols onto one or several transmission layers;

(iv) pre-coding of the complex-valued modulation symbols on each layer for transmission on the antenna ports;

(v) mapping of complex-valued modulation symbols for each antenna port to resource elements;

(vi) generation of complex-valued time-domain OFDM signal for each antenna port.

These operations are depicted and summarized in Figure 2. The details and implementation aspects of each block can be extracted from [4]. The transmitted signal in each slot is mapped onto a resource grid of N_a active subcarriers (frequency domain) and N_{symb} OFDM symbols (time domain). The number of OFDM symbols in a slot, N_{symb}, depends on
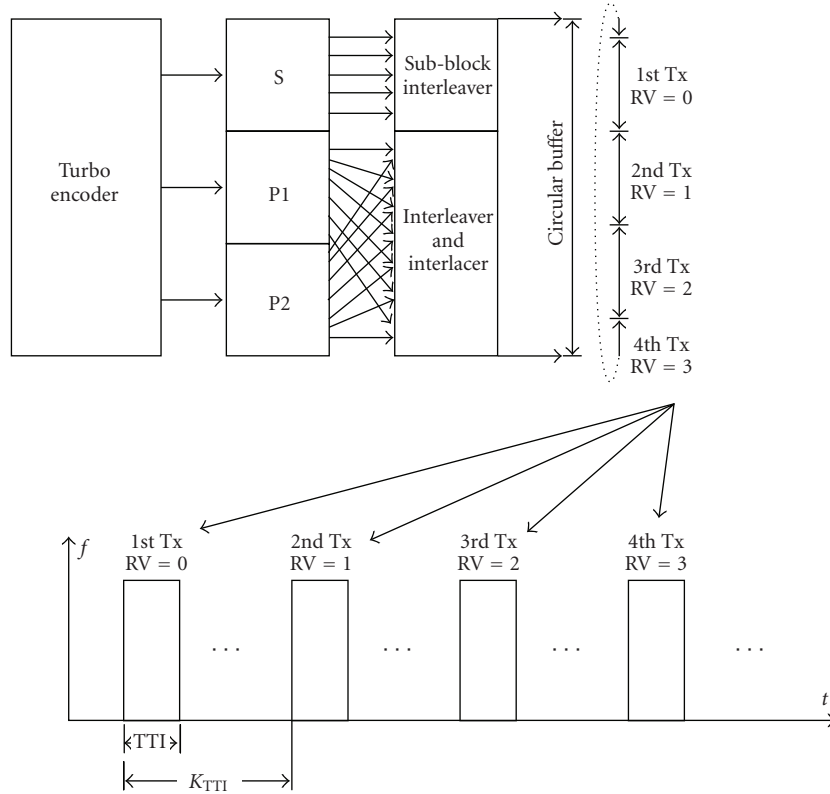
Figure 1: Rate matching and Virtual Circular Buffer.

the cyclic prefix length, N_{cp}, and the subcarrier spacing, Δf. In case of multiantenna transmission, there is one resource grid defined per antenna port. The size of the FFT/IFFT block, N_{FFT}, is equal to 2048 for $\Delta f = 15$ kHz and 4096 for $\Delta f = 7.5$ kHz. Finally, the time continuous signal of the generic ℓ-th OFDM symbol on the antenna port p can be written as

$$s_\ell^{(p)}(t) = \sum_{k=-\lfloor N_a/2 \rfloor}^{-1} a_{k+\lfloor N_a/2 \rfloor,\ell}^{(p)} e^{J2\pi k\Delta f(t-N_{cp}T_s)}$$
$$+ \sum_{k=1}^{\lceil N_a/2 \rceil} a_{k+\lfloor N_a/2 \rfloor-1,\ell}^{(p)} e^{J2\pi k\Delta f(t-N_{cp}T_s)} \tag{1}$$

for $0 \le t \le (N_{cp} + N_{FFT})T_s$ and where $a_{k,\ell}^{(p)}$ is a complex modulated symbol.

3. Adapting LTE to Satellite Links: Enablers

In the following sections, we propose and analyze some solutions to adapt the 3GPP LTE air interface to broadband satellite networks. These advanced techniques are applied to the transmitter or receiver side in order to enhance and maximize the system capacity in a mobile satellite environment.

3.1. Inter-TTI Interleaving. In this section, we propose an inter-TTI interleaving technique allowing to break channel

correlation in slowly varying channels, achieved through the reuse of existing H-ARQ facilities provided by the physical layer of the LTE standard [8].

The LTE standard does not foresee time interleaving techniques outside a TTI [7]. Thus, since the physical layer codeword is mapped into one TTI, the maximum time diversity exploitable by the Turbo decoder is limited to one TTI (T_{TTI}). For low to medium terminal speeds, the channel coherence time is larger than T_{TTI}, thus fading events cannot be counteracted by physical layer channel coding. In order to cope with such a fading events, LTE exploits both "intelligent" scheduling algorithms based on the knowledge of channel coefficients both in the time and in the frequency dimension, and H-ARQ techniques. The former technique consists in exploiting the channel state information (CSI) in order to map data into sub-carriers characterized by high signal to noise ratio (good channel quality). Of course this technique shows great benefits when frequency diversity is present within the active subcarriers.

H-ARQ consists in the "cooperation" between FEC and ARQ protocols. In LTE, H-ARQ operation is performed by exploiting the virtual circular buffer described in Section 2. Orthogonal retransmissions can be obtained by setting the RV number in each retransmission, thus transmitting different patterns of bits within the same circular buffer. Of course, H-ARQ technique yields to great performance improvement when time correlation is present because retransmission can have a time separation greater than channel coherence time.
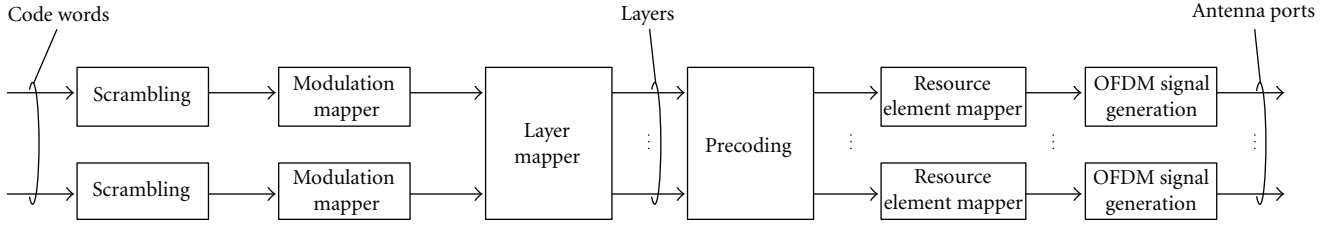
FIGURE 2: Overview of physical channel processing [4].

Unfortunately, neither of the aforementioned techniques can be directly applied to the satellite case due to the exceedingly large transmission delays, affecting both the reliability of the channel quality indicators and of the acknowledgements. Nevertheless, it is possible to devise a way to exploit the existing H-ARQ facilities adapting them to the satellite use. To this aim, we propose a novel forced retransmission technique, which basically consists in transmitting the bits carried in the same circular buffer within several TTIs, that acts as an inter-TTI interleaving. To do this, we can exploit the same mechanism as provided by the LTE technical specifications for the H-ARQ operations with circular buffer. For the explanation of this solution, the block diagram depicted in Figure 1 can be taken as reference. In this example, 4 retransmissions are obtained by using 4 different RVs, starting from 0 up to 3. Each of the 4 transmission bursts is mapped into different TTIs, spaced by $K_{TTI} \cdot T_{TTI}$. K_{TTI} is a key parameter because it determines the interleaving depth and it should be set according to channel conditions and latency requirements.

It is straightforward to derive the maximum time diversity achievable by adopting such as technique. Let R_{TTI} be the number of retransmissions needed to complete the transmission of a single circular buffer, L_{SUB} the number of OFDM symbols transmitted in each retransmission, and T_{SUB} the duration of L_{SUB} OFDM symbols. (The duration of the OFDM symbol T_{OFDM} is intended to be the sum of the useful symbol and cyclic prefix duration.) We have that a codeword is spread over total protection time $T_{TPT} = K_{TTI} \cdot (R_{TTI} - 1) \cdot T_{TTI} + T_{TTI}$. Given the fact that the standard facilities are used, no additional complexity is introduced. The drawback involved with the use of such technique is the data rate reduction, brought about by the fact that one codeword is not transmitted in T_{TTI} but in T_{TPT}. A possible way to maintain the original data rate is to introduce in the terminals the capability of storing larger quantities of data, equivalent to the possibility to support multiple H-ARQ processes in terminals designed for terrestrial use. In this way, capacity and memory occupation grow linearly with the number of supported equivalent H-ARQ processes, and is upper bounded by the data rate of the original link without inter-TTI.

3.2. PAPR Reduction Techniques. The tails in Peak-to-Average Power Ratio (PAPR) distribution for OFDM signals are very significant, and this implies an detrimental source of distortion in a satellite scenario, where the on-board

amplifier is driven near saturation. To have an idea of the cumulative distribution of PAPR, a Gaussian approximation can be used. With this approach, if OFDM symbols in time domain are assumed to be Gaussian distributed, their envelope can be modeled with a Rayleigh distribution. Thus, the cumulative distribution function of PAPR variable is

$$\mathbb{P}[\text{PAPR} \leq \gamma] = (1 - e^{-\gamma})^{N_{FFT}}. \quad (2)$$

A more meaningful measure is given by the *complementary cumulative distribution function*, which gives the probability that PAPR exceeds a given value γ, and can be written as

$$\mathbb{P}[\text{PAPR} \geq \gamma] = 1 - (1 - e^{-\gamma})^{N_{FFT}}. \quad (3)$$

As an example of using this simple approximation, which becomes increasingly tight increasing the FFT size, it is easy to check that a PAPR of 9 dB is exceeded with a probability of 0.5 assuming $N_{FFT} = 2048$, while a PAPR of 12 dB is exceeded with a probability of $2.7 \cdot 10^{-4}$.

This argument motivates the use of a PAPR reduction technique, in order to lower the PAPR and drive the satellite amplifier with a lower back-off. Power efficiency is at a prime in satellite communications, and an eventual reduction of the back-off implies an improvement in the link budget and an eventual increase of the coverage area. Amongst all requisites for PAPR reduction techniques (see [9, 10] for a general overview), the compatibility with the LTE standard is still fundamental. Secondly, the receiver complexity must not be significantly increased. Furthermore, no degradation in BER will be tolerated, because it would require an increased power margin. Finally, the PAPR reduction method will cope with the severe distortion given by the satellite: even if the amplifier has an ideal pre-distortion apparatus on-board, it is operated near to its saturation, where a predistorter could not invert the flat HPA characteristic. The cascade of an ideal predistorter and the HPA is the so-called *ideal clipping* or *soft limiter*. In such a scenario, if the PAPR is lower than the IBO the signal will not be distorted, while if the PAPR is significantly higher the signal will be impaired by non-linear distortion. Thus, the PAPR reduction technique should offer a good PAPR decrease for almost all OFDM symbols, rather than a decrease which can be experienced with a very low probability.

Several techniques have been proposed in the literature, and even focusing on techniques which do not decrease the spectral efficiency, the adaptation to satellite scenario remains an issue: this is the case of *Tone Reservation* [11–13], the intermodulation products of satellite amplifier

prevent using this technique, while it is very popular in the wired scenario and when the amplifier is closer to its linear region. The *Selected Mapping* technique [14, 15], although easy and elegant, needs a *side information* at the receiver. The side information can be avoided, at expense of a significant computational complexity increase at the receiver. Companding techniques (see [10] and references therein) offer a dramatic reduction in PAPR and do not require complex processing. On the other hand, there is a noise enhancement, which turns out to be an important source of degradation at the very low SNRs used in satellite communications.

The *Active Constellation Extension* (ACE) technique [16] fulfills those requirements, moreover the power increase due to PAPR reduction is exploited efficiently, obtaining an additional margin against noise. The ACE approach is based on the possibility to dynamically extend the position of some constellation points in order to reduce the peaks of the time domain signal (due to a constructive sum of a subset of the frequency domain data) without increasing Error Rate: the points are distanced from the borders of their Voronoi regions. The extension is performed iteratively, according to the following procedure.

(1) Start with the frequency domain representation of a OFDM symbol.

(2) Convert into the time-domain signal, and clip all samples exceeding a given magnitude V_{clip}. If no sample is clipped, then exit.

(3) Reconvert into the frequency domain representation and restore all constellation points which have been moved towards the borders of their Voronoi regions.

(4) Go back to 2 until a fixed number of iteration is reached.

This algorithm is applied to data carriers only, excluding thus pilots, preamble/signalling and guard bands. In the performance evaluation of the algorithm, the amplitude clipping value is expressed in term of the corresponding PAPR, which is called *PAPR-Target* in the following.

The most critical point of this method is the choice of the clipping level V_{clip}: a large value for V_{clip} (which corresponds to an high *PAPR-Target*) will yield a negligible power increase and a poor convergence, since signal is unlikely to be clipped. On the opposite extreme, a very low clipping level will yield again a poor convergence and a negligible power increase. In fact, considering the above algorithm, almost all points will be moved by clipping in *step-2* and then restored by the constellation constraint enforcing in *step-3*. A compromise value, which will lead to a PAPR around 5 or 6 dB is advisable, yielding a good convergence and a slight energy increase, due to the effectiveness of the extension procedure. Although there are other ACE strategies [16], the solution presented here is attractive because it can be easily implemented both in hardware and software, as reported in [17].

3.3. Random Access Signal Detection. The Random Access Channel (RACH) is a contention-based channel for initial uplink transmission, that is, from mobile user to base station. While the Physical RACH (PRACH) procedures as defined in the 3G systems are mainly used to register the terminal after power-on to the network, in 4G networks, PRACH is in charge of dealing with new purposes and constraints. In an OFDM based system, in fact, orthogonal messages have to be sent, thus the major challenge in such a system is to maintain uplink orthogonality among users. Hence both frequency and time synchronization of the transmitted signals from the users are needed. A downlink broadcast signal can be sent to the users in order to allow a preliminary timing and frequency estimation by the mobile users, and, accordingly a timing and frequency adjustment in the return link. The remaining frequency misalignment is due to Doppler effects and cannot be estimated nor compensated. On the other hand, the fine timing estimation has to be performed by the base station when the signals coming from users are detected. Thus, the main goal of PRACH is to obtain fine time synchronization by informing the mobile users how to compensate for the round trip delay. After a successful random access procedure, in fact, the base station and the mobile user should be synchronized within a fraction of the uplink cyclic prefix. In this way, the subsequent uplink signals could be correctly decoded and would not interfere with other users connected to the network.

PRACH procedure in 4G systems consists in the transmission of a set of preambles, one for mobile user, in order to allocate different resources to different users. In order to reduce collision probability, in the LTE standard, Zadoff-Chu (ZC) sequences [18], known also as a Constant Amplitude Zero Autocorrelation (CAZAC) sequences, are used as signatures between different use, because of the good correlation properties. The ZC sequence obtained from the u-th root is defined by

$$x_u(n) = \exp^{-j(\pi u n(n+1)/N_{ZC})} \quad 0 \le n \le N_{ZC} - 1, \quad (4)$$

where N_{ZC} is the preamble length in samples and it has been set to 839. ZC sequences present very good autocorrelation and cross-correlation properties that make them perfect candidates for the PRACH procedure. In fact, orthogonal preambles can be obtained cyclic rotating two sequences obtained with the same root, according to the scheme shown in Figure 3 and the expression

$$x_{u,v}(n) = x_u((n + C_v) \bmod N_{ZC}) \quad v = 0, 1, \ldots, \left\lfloor \frac{N_{ZC}}{N_{CS}} \right\rfloor - 1, \quad (5)$$

where N_{CS} is the number of cyclic shifts. It can be easily verified that the cross correlation function presents N_{CS} peaks and N_{CS} zero correlation zones. Figure 4(a) shows a magnification of the cross correlation function for different shifts considering $N_{CS} = 64$. It will be noted that there are $N_{CS} - 2$ zero correlation zones with length equal to 12 samples and the last zero correlation zone with 20 samples. Preambles obtained from different roots are no longer orthogonal but, nevertheless, they present good correlation properties.

Considering a 4G system via satellite, the number of users to be allocated in each cell depends on the system
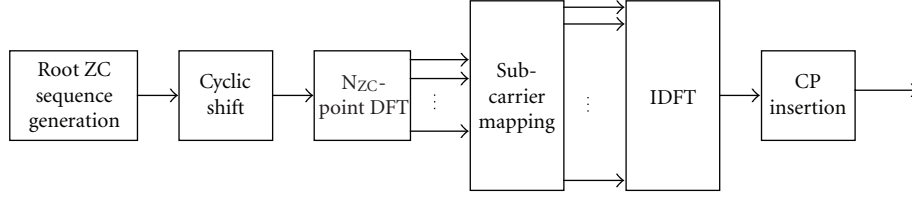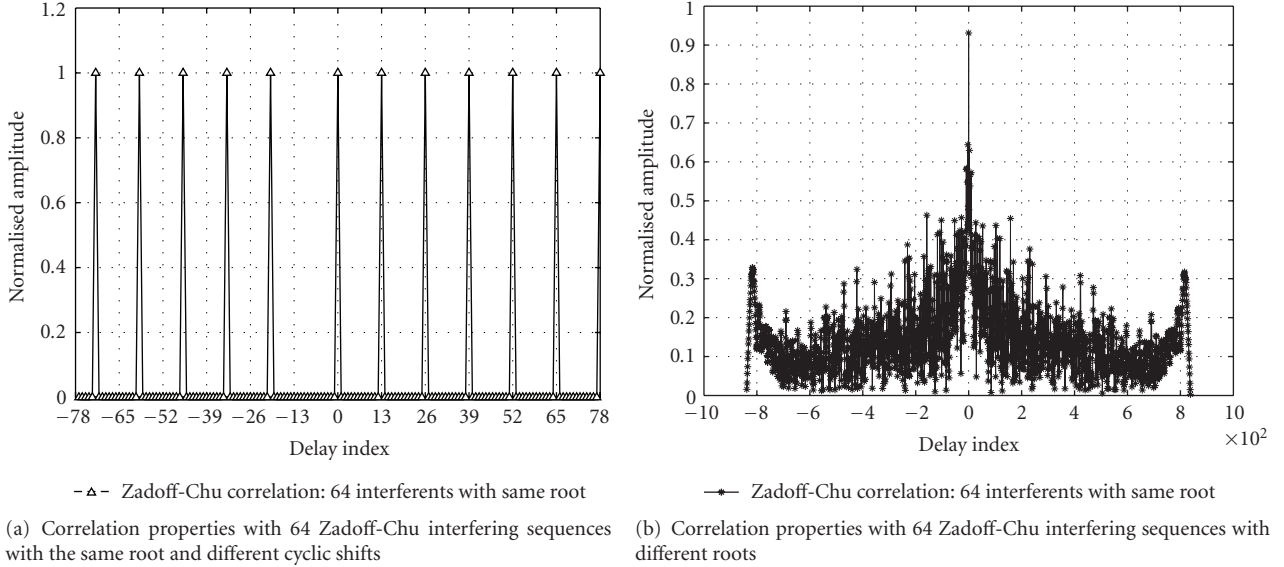
FIGURE 3: ZC generation in time domain processing.

- △ - Zadoff-Chu correlation: 64 interferents with same root

(a) Correlation properties with 64 Zadoff-Chu interfering sequences with the same root and different cyclic shifts

- * - Zadoff-Chu correlation: 64 interferents with same root

(b) Correlation properties with 64 Zadoff-Chu interfering sequences with different roots

FIGURE 4: Detection properties in the presence of interferers.

TABLE 1: ZC allocation for GEO satellite scenario.

Cell Radius [km]	Number of root ZC sequences	Number of cyclic shift per root sequence
150 (Near polar arctic circle)	64	1
300 (Near polar arctic circle)	64	1
500 (Near polar arctic circle)	64	1
150 (Europe)	64	1
300 (Europe)	64	1
500 (Europe)	64	1
150 (Tropical)	32	2
300 (Tropical)	64	1
500 (Tropical)	64	1
150 (Equator)	2	32
150 (Equator)	8	8
150 (Equator)	16	4

design. The zero correlation zone of the preambles has to be larger then the maximum round trip propagation delay, depending on cell radius and multipath delay. The number of root ZC sequences and the number of cyclic shift sequences depend on cell radius and on the geographical position, and they are reported in Table 1 for GEO satellites. Note that

the worst case corresponds to the presence of 64 sequences obtained from different roots. In this case, the satellite has to detect each sequence even between the interference from the others. Figure 4(b) shows the correlation function in a scenario like this, and it is worthwhile noting that the peak can once more be detected, also in the presence of 63 interferers. Detection performance in terms of Receiver Operating Characteristics (ROC), that is, Missed Detection Probability (P_{md}) as a function of False Alarm Probability (P_{fa}) have been reported for different numbers of interferers in Figure 5. It will be highlighted that the detection has been performed in the frequency domain and a Non-Coherent Post-Detection Integration (NCPDI) [19] scheme has been adopted. Finally, the results are shown in a AWGN scenario with a signal to noise ratio, E_s/N_0, equal to 0 dB.

4. Upper Layer FEC Analysis

In this section, we propose a UL-FEC technique working on top of the PHY layer. It is well known that channel coding can be performed at different layers of the protocol stack. Two are the main differences which arise when physical layer or upper layer coding is addressed: the symbols composing each codeword, and the channel affecting the transmitted codeword. Indeed, at physical layer the symbols involved in the coding process typically belong to the Galois Field of
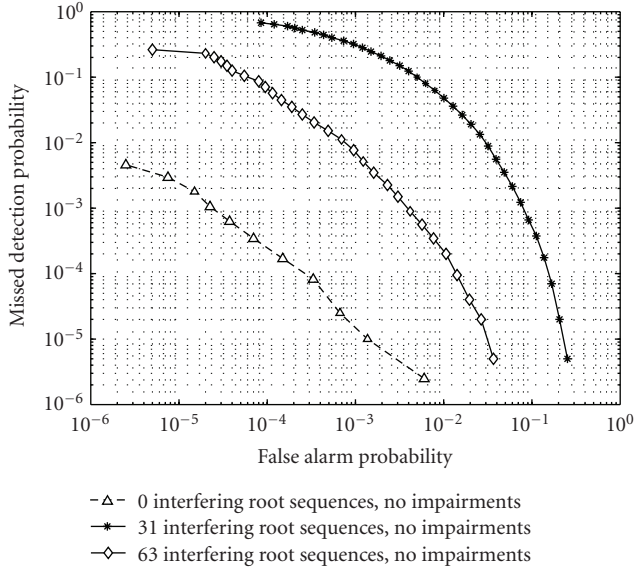
FIGURE 5: ROC in AWGN channel with $E_s/N_0 = 0.0$ dB without interference, and with interferers with different roots.

order m, $GF(m)$. Nevertheless, also non binary codes can be adopted. Working at upper layer each symbol composing the UL codeword can be made up of packets of bits, depending on the application level.

In order to build the UL-FEC technique on solid ground, the design and analysis has been carried out starting from the Multi Protocol Encapsulation Forward Error Correction Technique (MPE-FEC) adopted by the DVB-H standard [20], and successively enhanced and modified in the framework of the DVB-SH [1] standardization group. With respect to the MPE-FEC approach, the implementation of the UL-FEC technique for this framework has required to adapt the parameter setting to the LTE physical layer configurations. In the following, we adopt this terminology:

(i) k: the UL block length, that is the number of systematic symbols to be encoded by the UL encoder

(ii) n: the UL codeword length, that is the number of UL symbols produced by the UL encoder

(iii) k': the actual UL-FEC block length if zero-padding is applied

(iv) n': the actual UL-FEC codeword length if zero-padding and/or puncturing is applied

(v) N_{JCC}: number of jointly coded channels at physical layer

(vi) S_{JCC}: size of each channel in bytes

(vii) S_{UL-CRC}: size of the upper layer Cyclic Redundancy Check (CRC) in bytes

(viii) $S_{PHY-CRC}$: size of the physical layer CRC in bytes

(ix) K_{PHY}: physical layer block length in bytes.

As in MPE-FEC, we define the UL-FEC matrix as a matrix composed of a variable number of rows (n_of_rows) and n

columns. Each entry of the matrix is an UL-symbol, that is, 1 byte. The first k columns represent the systematic part of the matrix and are filled with the systematic UL-symbols coming from the higher level. The last $n - k$ columns carry the redundancy data computed on the first k columns. It is worthwhile to notice that the n and k values depend on the selected UL code rate only, while n_of_rows is a parameter chosen accordingly to the physical layer configuration and is set by using the following formula: $n\_of\_rows = K_{PHY} - S_{PHY-CRC} - N_{JCC}S_{UL-CRC}$. As a consequence, the number of bytes available for each channel in a given UL-FEC matrix column is $S_{JCC} = n\_of\_rows/N_{JCC}$. With this configuration, the following operations must be sequentially performed.

(1) The information data coming from higher layer are written columns-wise in the systematic data part of the UL-FEC matrix.

(2) A Reed-Solomon (RS) encoding (n, k) is performed on each row producing the redundancy part of the UL-FEC matrix.

(3) The data are transmitted column-wise.

(4) An UL-CRC is appended after each group of S_{JCC} bytes.

(5) Each group of $K_{PHY} = N_{JCC}(S_{JCC} + S_{UL-CRC})$ bytes composes a physical layer information packet.

(6) The PHY-CRC is appended to each physical layer information packet according to the LTE specifications [7].

For sake of simplicity, we adopt the same RS mother code provided in [20], which is an RS(255,191). The code rate of this mother code is 3/4. Further code rates can be achieved by using padding or puncturing techniques. For instance, if a UL-FEC rate 1/2 is needed, zero-padding is performed over the last 127 columns of the systematic data part of the UL-FEC matrix, yielding to $k' = 64$ and $n' = 128$. The choice of this RS code allows fully compatibility with DVB-H networks.

It is important to note how the application of the CRC at UL and physical layer has an impact on the overall system performance. To better evaluate this impact, we distinguish to study cases:

(i) *Case-A*: only the PHY-CRC is considered ($S_{UL-CRC} = 0$). In this scenario, the receiver is not able to check the integrity of a single UL packet carried within the same physical layer information packets. This basically means that if error is detected in the physical layer information packet, all UL packets will be discarded;

(ii) *Case-B*: both PHY and UL CRC are applied.

It is quite obvious that *Case-B* outperforms *Case-A*. In fact, if only a small fraction of bits are wrong after physical layer decoding, *Case-B* is able to discard only the UL packets in which erroneous bits are present, while *Case-A* discards all N_{JCC} carried within the physical layer information packets. The price to pay is an increased overhead of *Case-B* with respect to *Case-A* due to the extra CRC bits appended.

At the receiver side, depending whether *Case-A* or *Case-B* is taken into account, CRC integrity must be performed at different levels. If the *Case-A* is considered, only the CRC at physical layer determines the data reliability; whereas in the *Case-B*, the PHY-CRC could be ignored and the data reliability is only determined by the UL-CRC. Then, the UL-FEC matrix is filled with the reliable data. In particular, for the *Case-A* an entire column is marked as reliable or not reliable, while in the *Case-B* the UL-FEC matrix columns could be partially reliable. Finally, the RS(n, k) decoding is performed on each row. If the number of reliable position in a row is at least k, the decoder is able to successfully decode the received information, and all unreliable positions are recovered.

The UL-FEC protection capability against burst of errors can be characterized by the so-called Maximum Tolerable Burst Length (MTBL) [21], which consists in the maximum time protection that the UL-FEC technique can provide. The MTBL depends on both UL-FEC parameters and PHY data rate. In our proposal one PHY information packet is mapped in one column of the UL-FEC matrix. Since we are dealing with MDS codes, the decoder is able to successfully decode if at least k' columns are correctly received in the UL-FEC matrix. Thus, the MTBL is simply given by the time taken by transmitting $n' - k'$ columns, that is, the duration of $n' - k'$ information packets. The MTBL can be increased by adopting a sliding encoding mechanism [22]. The sliding encoding is a UL interleaver mechanism: a UL-FEC encoder implementing sliding encoding selects the k' data columns from a window (SW) among the UL-FEC matrices and spreads the $n' - k'$ parity sections over the same window. Basically, the same effect could be obtained by first normally encoding SW frames and then interleaving sections among the encoded SW frames. The total protection time TPT_{UL} achievable at upper layer by means of such a technique is given by $\text{TPT}_{\text{UL}} = n' \cdot \text{SW} \cdot T_{\text{TTI}}$.

5. Simulation Results

Here, we discuss separately the numerical results obtained by implementing the solutions presented in Section 3. The following general assumptions have been considered during the implementation of all techniques.

The LTE transmitted signal occupies 5 MHz of bandwidth, $N_a = 300$, located in S-band (central frequency $f_0 = 2$ GHz), the sub-carrier spacing is $\Delta f = 15$ kHz, and FFT/IFFT size is fixed to $N_{\text{FFT}} = 2048$. The long cyclic prefix is assumed, $N_{\text{cp}} = 512$, thus $N_{\text{symb}} = 12$ OFDM symbols are transmitted in each TTI. The resulting OFDM symbols duration is $T_{\text{ofdm}} = 83.33 \, \mu$s, including the cyclic prefix duration of $T_{\text{cp}} = 16.67 \, \mu$s.

5.1. Inter-TTI Improvements. For evaluating the inter-TTI proposal, the turbo encoder is fed with 2496 information bits, while the circular buffer size is assumed to be 6300, thus resulting in an actual system code rate equal to $R \simeq 2/5$. All simulations have considered QPSK modulation.
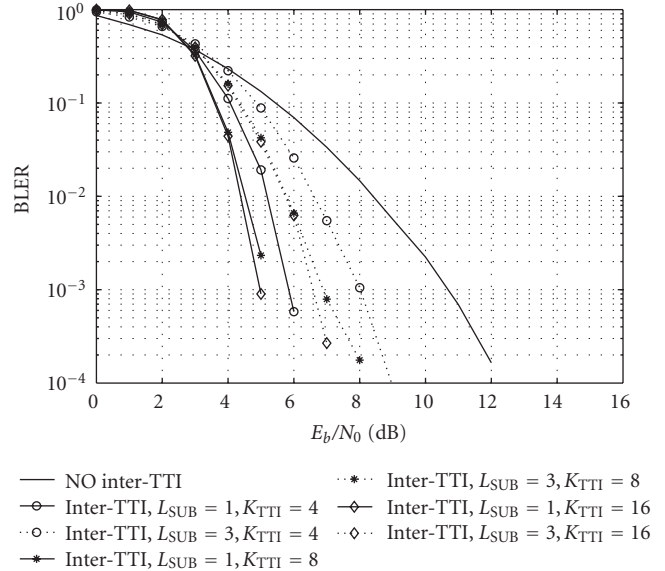

FIGURE 6: BLER versus E_b/N_0. Terminal speed is equal to 30 km/h.

Figure 6 shows the block error rate (BLER) performance versus E_b/N_0, with E_b being the energy per information bit and N_0 the one-sided noise power spectral density. The curves refer to a user terminal speed of 30 km/h. The solid line curves represent the cases in which the number of transmitted OFDM symbols for each retransmission (L_{SUB}) is 1, resulting in a total number of retransmissions $R_{\text{TTI}} = 12$, while the dashed line curves depict the case with $L_{\text{SUB}} = 3$ and $R_{\text{TTI}} = 4$. In these configurations, we set the value of K_{TTI} such that the total protection time T_{TTI} is larger than the channel coherence time T_c, which for these simulations is about $T_c \simeq 9$ ms. (This is the coherence time of the small scale fluctuations, and it depends directly from the terminal speed and the central carrier frequency.) In particular, the simulated values K_{TTI} are 4, 8, 16. As it can be observed, the solid line curves always outperform the dashed line ones. This is easily explained considering the different diversity granularity: in the case of $L_{\text{SUB}} = 1$, each OFDM symbol is transmitted in a separated TTI. Therefore, the codeword spanned over the 12 OFDM symbols composing the entire TTI can benefit of diversity degree equal to 12. On the other hand, if the case of $L_{\text{SUB}} = 3$ is considered, the degree diversity is reduced to 4. It is worthwhile to note the large performance enhancement yielded by the adoption of the inter-TTI technique. For instance, looking at Figure 6, the performance gain at BLER $= 10^{-3}$ increases up to 6 dB in the case of $L_{\text{SUB}} = 1$, and up to 4 dB considering $L_{\text{SUB}} = 3$.

5.2. ACE Performance. The results of the ACE algorithm for PAPR reduction are discussed. First of all, the CCDF of PAPR distribution have been analyzed for verifying the effectiveness of the selected method.

Figures 7 and 8 show PAPR distribution for QPSK and 16QAM, respectively. As it can be seen, if the *PAPR-Target* is too low, the CCDF curve has a poor slope. Increasing the *PAPR-Target*, the curve is shifted left until
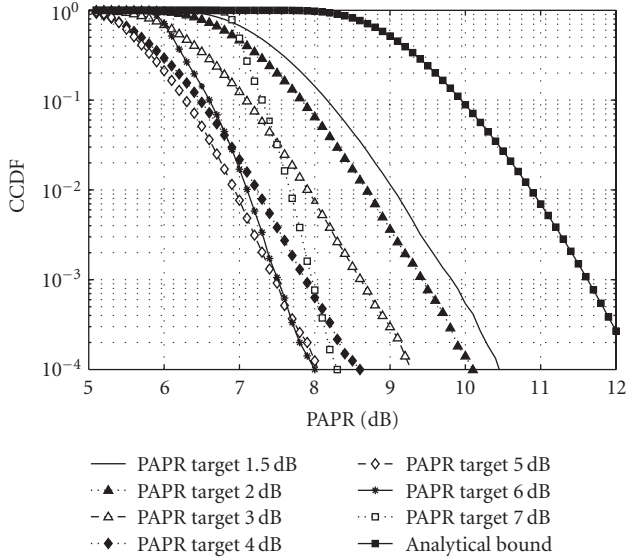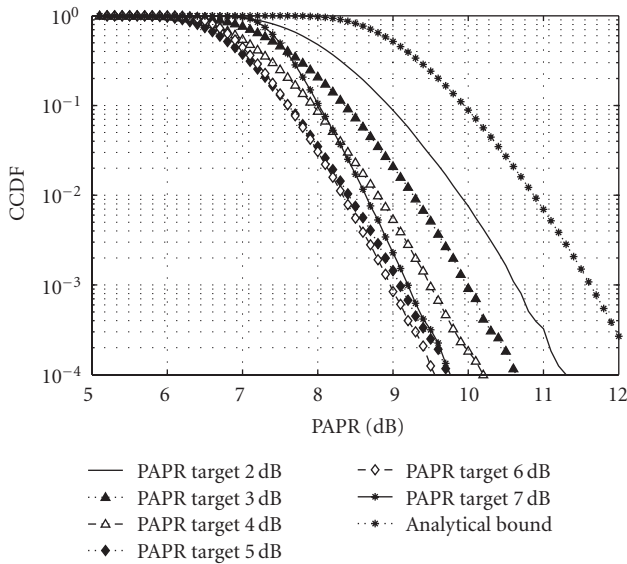
FIGURE 7: PAPR CCDF with QPSK modulation.

FIGURE 8: PAPR CCDF with 16QAM modulation.

FIGURE 9: BER performance using PAPR techniques with 16QAM and code-rate = 3/5.

a certain value, then the steepness increases and, if the *PAPR-Target* is furthermore increased, the curve is shifted right, maintaining the same steepness. This phenomenon is more evident for QPSK modulation rather than for 16QAM, and this difference can be explained considering that all QPSK constellation points can be moved in some directions by the ACE algorithm, while for 16QAM the inner points must be immediately restored, and the points on the edges have only one degree of freedom.

A more interesting figure of merit related to this PAPR reduction technique is the improvement in terms of bit error rate, which summarizes the impact of PAPR reduction on the end-to-end performance. Figure 9 shows the BER improvement in a frequency selective channel, with the
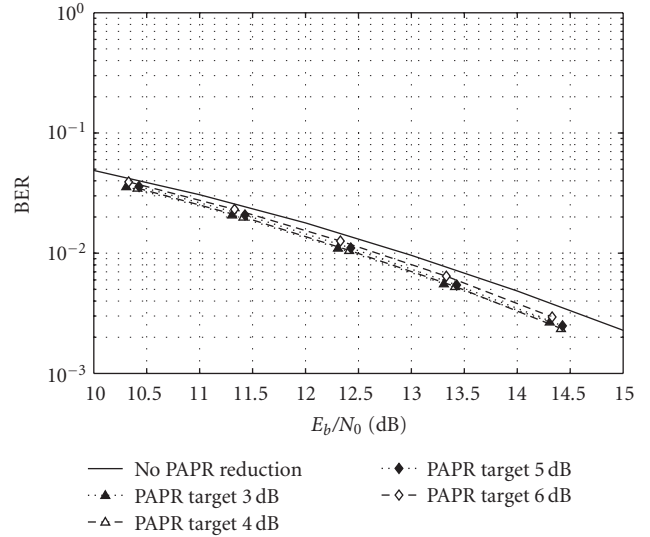
amplifier Input Back-Off (IBO) set to 3 dB. The 16QAM modulation is considered, the coding rate is $r = 3/5$, and the packet size is chosen equal to 7552 bits. As shown in Figure 9, there is a gain of almost 0.5 dB if the *PAPR-Target* is kept low; the gain is slightly lower if the *PAPR Target* is chosen in order to maximize the beneficial effects of ACE technique in terms of PAPR CCDF. This result can be justified by considering the worst-case conditions assumed in these simulations: the amplifier driven 3 dB far from saturation requires a PAPR value as low as possible, while the slight energy increase is conveniently exploited in such a severe fading channel environment.

5.3. Redundancy Split Analysis. A comparison between the UL-FEC and the inter-TTI interleaver technique is reported. In order to make a fair comparison between these two techniques, in the following we keep constant the overall spectral efficiency by distributing the redundancy between UL-FEC and physical layer. Figure 10 shows the numerical results obtained in the case of assuming the terminal speed equal to 3 km/h, and ideal channel estimation. The performance is measured in terms of BLER versus E_b/N_0. All reported curves have a spectral efficiency equal to 4/5 bit/s/Hz. In the inter TTI case, we have considered the coding rate $r = 2/5$ and QPSK modulation, and we have varied both the interleaver depth and the subframe size. On the other hand, the UL-FEC solution have been implemented by considering $r = 4/5$ with QPSK modulation at the physical layer, and the $(k' = 64, n' = 128)$ code at the upper layer. Since the considered UL-FEC protection spans over $n' = 128$, that corresponds to 128 ms, the most comparable protection time provided by the inter-TTI approach is obtained by adopting the parameters $K_{TTI} = 40$ and $L_{SUB} = 3$, which still guarantee orthogonal retransmissions. In this case, the physical layer codeword spans over $K_{TTI} \cdot 4 = 160$ TTIs, that is, 160 ms. From the analysis of the results, we can state that on the
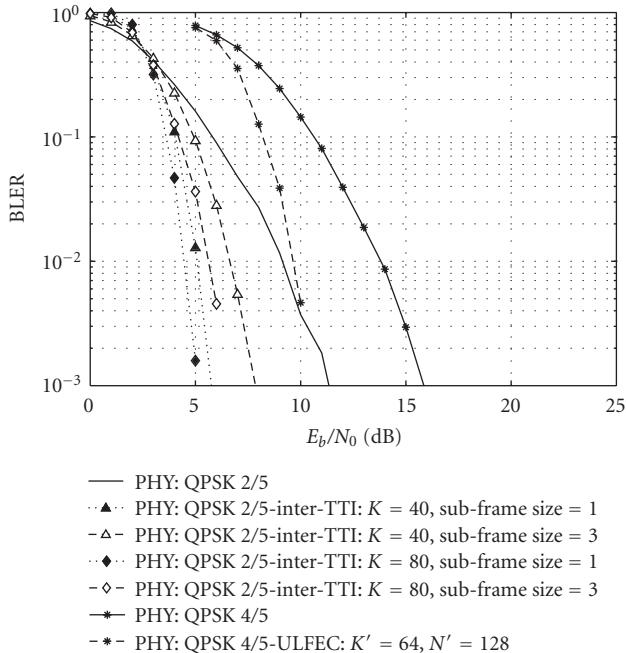
FIGURE 10: Comparison between Inter-TTI and UL-FEC techniques.

one hand, the inter TTI techniques outperforms the UL-FEC technique, which can be justified recalling that at physical layer the decoder can exploit soft information, thus achieving much better performance with respect to the hard decoding performed at upper layer. On the other hand, the inter-TTI technique requires a large memory buffer at the output of the base-band processor. A through complexity analysis must be carried out to this respect in order to understand the hardware feasibility of the assumption considered for the inter-TTI interleaving case.

5.4. End-to-End Performance Evaluation. In this section, the results obtained considering end-to-end simulations in realistic satellite propagation scenario are analyzed. To this aim, we have adopted the Land Mobile Satellite (LMS) channel model proposed in [23], which is based on measurement campaigns. This channel model is characterized by a three states Markov model. Each state describes different propagation conditions, that are line of sight, moderate shadowing conditions, and deep shadowing conditions. By suitably setting the Markov chain parameters, several environment can be modeled. In our analysis we have considered an elevation angle of 40 degrees and the following environments: open area [O], Suburban [S], Intermediate tree shadow [ITS], Heavy Tree Shadow [HTS]. Such environments are characterized by long fading events due to the superposition of shadowing effects. It is quite obvious that applying the proposed UL-FEC technique without any interleaver working at UL does not allow to cope with such channel impairments. Indeed, the MTBL achievable by adopting UL-FEC without sliding interleaving (SW = 1) is in the order of hundreds milliseconds. To increase the MTBL

we adopt the sliding window encoding technique. As already mentioned, this technique basically consists in applying a block interleaver at UL.

In order to correctly evaluate the achievable performance of the proposed UL-FEC technique, we have fed the UL-FEC decoder with time series. Since the fading is frequency flat and for low to medium terminal speeds time selectivity is negligible with respect to the TTI duration (channel coherence time equal to 9 ms at 30 km/h, whereas TTI duration equal to 1 ms for LTE), we can assume that the SNR is constant within the whole TTI (both in frequency and in time). (Again, this fading coherence time is referred to the small scale fluctuations, while the large scale is taken into account in the LMS channel parameters.) Under these assumptions, the BLER time series can be generated using a simplified method, that does not require the actual simulation of the whole physical layer chain. The adopted procedure is depicted in Figure 11, and is made up by the following steps:

(1) perform AWGN simulations (including NL distortion), to obtain the function BLER versus E_b/N_0;

(2) generate the Perez Fontan channel coefficients, obtaining signal levels relative to LOS component;

(3) calculate the received C/N_0 value in LOS conditions;

(4) map the instantaneous C/N_0 value into E_b/N_0;

(5) generate the time series, producing a "1" (wrong block) or a "0" (correct block) according to the following algorithm: *if [uniform-random-variable < BLER $(E_b/N_0{}^*)$] then time-series-value = 1, else time-series-value = 0.*

In order to get a synthetic analysis of the results, we have assessed the Erroneous Seconds Ratio (ESR) criterion. The ESR was also considered by the DVB-SSP [24] group to be the most relevant performance parameter for the assessment of the impact on the video quality. In particular, we take into account the ESR5(20) criterion: ESR5(20) is fulfilled for a given time interval of 20 seconds if the percentage of erroneous seconds in the same time interval does not exceed 5%, which corresponds to a maximum of 1 erroneous second. The percentage of time satisfying the ESR5(20) criterion represents the "ESR5(20) fulfillment percentage." The conclusions of this analysis are summarized in Figure 12, where the achievable spectral efficiency is reported as a function of the C/N required to satisfy the ESR5(20) criterion at 90%. The spectral efficiency is computed considering the PHY configurations listed in Table 2. Notably, since usually in a LTE frame both information and control data are transmitted, we assumed that the equivalent of 1 OFDM symbol per TTI, that is, 1/12 of the TTI, is completely dedicated to the transmission of control data. As a consequence, the PHY spectral efficiency resulting from Table 2 has been reduced by a factor (11/12).

In Figure 12, each curve represents the performance of the QPSK constellation in a given scenario and for a given UL-FEC coding rate. The connected markers in each curve represent the corresponding PHY configurations in a given
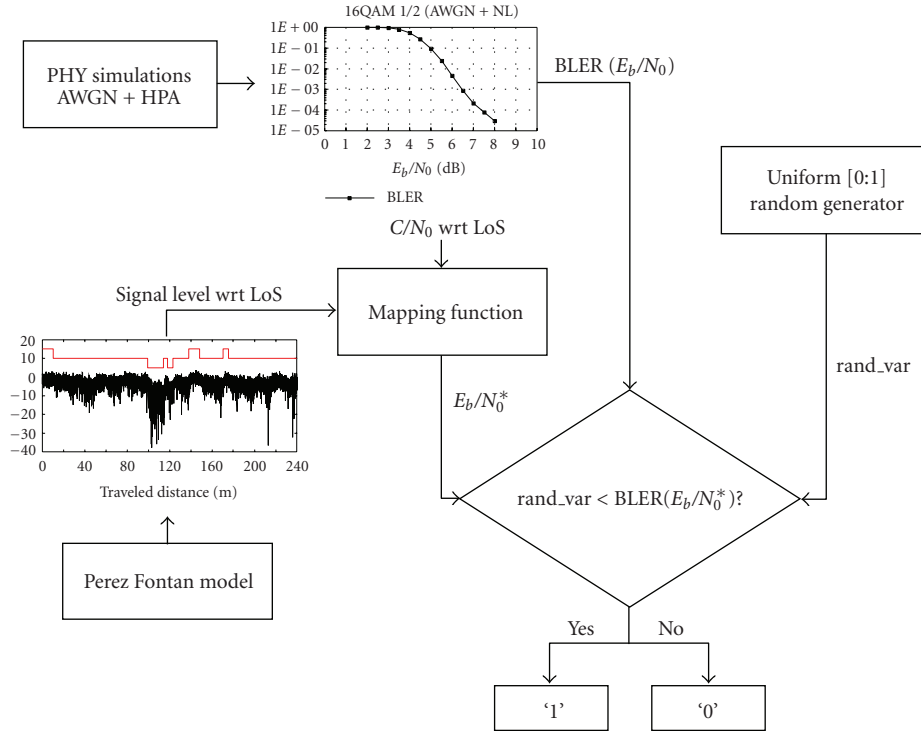
FIGURE 11: Block diagram of the procedure adopted for generating the time series.

TABLE 2: Adopted LTE Physical layer configurations.

Number of jointly coded channels/number of channel groups	Info-bits per packet	Allocated data carriers per sub-frame [RBs × OFDM symbols]	Modul.	FEC Code rate	Overall Bit Rate Channel
8/1	2496	3150 [25 × 12]	QPSK	2/5	2.50 Mb/s
16/1	4992	3150 [25 × 12]	QPSK	4/5	4.99 Mb/s
24/1	7552	3150 [25 × 12]	16QAM	3/5	7.49 Mb/s

scenario and for a given UL-FEC coding rate. Regarding the UL parameters, two configuration have been taken into account: rate 1/2 ($n' = 128$, $k' = 128$) and rate 3/4 ($n' = 191$, $k' = 255$). The adopted sliding window size has been set to SW = 101 for the rate 1/2 case, and 50 for the rate 3/4, yielding to a total protection time at UL equal to $\text{TPT}_{\text{UL}} = 12.928$ s, and $\text{TPT}_{\text{UL}} = 12.75$ s, respectively. Notably, for the 16QAM constellation, only one PHY FEC scheme has been considered. Interestingly, the lower UL-FEC protection, that is, 3/4, always outperforms, at the same total spectral efficiency, the higher UL-FEC protection, with the only exception of the Heavy Tree Shadow scenario. In that case, the extremely challenging propagation conditions calls in fact for a very strong protection along with a quite demanding link budget.

6. Conclusions and Recommendations

The adoption of the 3GPP LTE air interface to broadband satellite networks has been evaluated. The rationale for this choice was the maximization of the commonalities with the terrestrial air interfaces, so as to reduce both non-recurrent engineering and production costs, while easing interworking procedures. The selected numerologies for forward and reverse links are standard compatible. In this sense, the results produced are significant from the 3GPP point of view.

Regarding time domain fade mitigation techniques, one of the major findings consists in a way to obtain the above diversity in an almost standard compatible way. This is the inter-TTI technique, which has been shown to bring significant benefits without touching the physical layer definition.

PAPR reduction algorithms, coupled to predistortion techniques, are a novelty for OFDM transmission through a satellite. We have explored this architecture and our results show that the PAPR itself can be reduced by 2 to 4 dB (guaranteed at 99.9%), which translates into the possibility to reduce the OBO by about 0.7 dB and to gain about 0.5 dB in E_b/N_0 for typical quality of services. All in all, we can
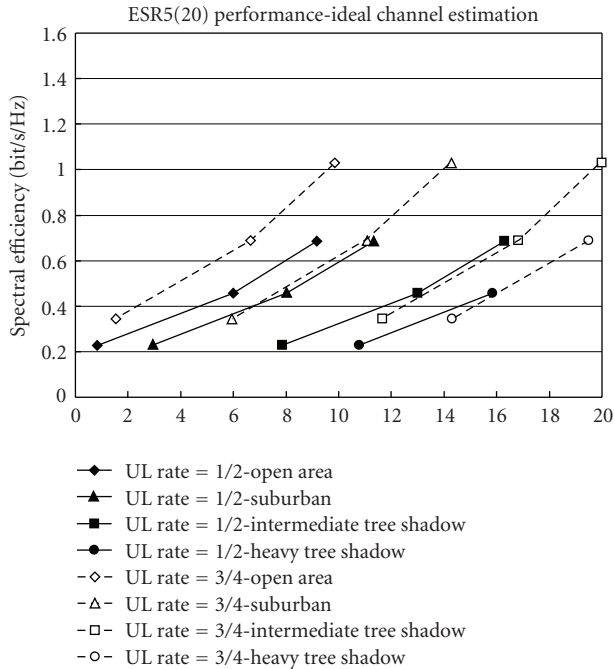
ESR5(20) performance-ideal channel estimation

FIGURE 12: Overall (PHY + UL) spectral efficiency versus *C/N* for 90% ESR5(20).

- ◆ — UL rate = 1/2-open area
- ▲ — UL rate = 1/2-suburban
- ■ — UL rate = 1/2-intermediate tree shadow
- ● — UL rate = 1/2-heavy tree shadow
- ◇ — UL rate = 3/4-open area
- △ — UL rate = 3/4-suburban
- □ — UL rate = 3/4-intermediate tree shadow
- ○ — UL rate = 3/4-heavy tree shadow

expect a gain in total degradation around 1 dB, which is certainly not negligible.

Regarding frame acquisition procedures, they are quite specific for LTE air interface. The design of acquisition sequences for 3GPP LTE has been performed adapting it to the different requirements set by satellite transmission involving the use of large geographic beams.

Additionally, in order to further extend the link reliability over the satellite link, the use of UL-FEC techniques has been investigated. Simulation results clearly show that the UL-FEC technique is a very effective solution that can drastically improve the achievable block error rate and ESR5(20) performance.

In order to provide useful guidelines for the system design, the analysis of the optimum redundancy split between physical and upper layer coding has been performed. In this case, results show that in most cases it is beneficial to limit the protection at physical layer in order to ease channel estimation and to compensate the reduced performance through a stronger UL coding. The rationale behind this conclusion is that the UL-FEC benefits a larger time diversity thus performing significantly better than the physical layer coding in almost all scenarios.

Acknowledgment

References

[1] ETSI EN 302 583, "Digital video broadcasting (DVB); framing structure, channel coding and modulation for satellite services to handheld devices (SH) below 3 GHz," v1.1.1, March 2008.

[2] The Integral Satcom Initiative (ISI), "ISI strategic research agenda," FP7 Technology Platform, v1.1, January 2006, http://www.isi-initiative.eu.org/isi_joomla.

[3] ETSI TR 102 443, "Satellite earth stations and systems (SES); satellite component of UMTS/IMT-2000; evaluation of the OFDM as a satellite radio interface," v1.1.1, August 2008.

[4] 3GPP TS36.211, "3rd Generation Partnership Project; Technical Specification Group Radio Access Network; Evolved Universal Terrestrial Radio Access (E-UTRA); Physical Channels and Modulation (Release 8)," v8.2.0, March 2008.

[5] "IEEE standard for local and metropolitan area networks, part 16: air Interface for fixed and mobile broadband wireless access systems amendment 2: physical and medium access control layers for combined fixed and mobile operation in licensed bands and corrigendum 1," IEEE Computer Society and the IEEE Microwave Theory and Techniques Society, 20 February 2006.

[6] G. E. Corazza, P. Britten, I. Buret, et al., "Defining the role of satellite communications in 4G," in *Proceedings of the 8th World Wireless Congress on Fourth Generation Mobile Communications (WWC '07)*, pp. 60–64, San Francisco, Calif, USA, May 2007.

[7] 3GPP TS36.212, "3rd Generation partnership project; technical specification group radio access network; evolved universal terrestrial radio access (E-UTRA); multiplexing and channel coding (release 8)," v8.2.0, March 2008.

[8] M. Papaleo, M. Neri, G. E. Corazza, and A. Vanelli-Coralli, "Using LTE in 4G satellite communications: increasing time diversity through forced retransmission," in *Proceedings of the 10th International Workshop on Signal Processing for Space Communications (SPSC '08)*, Rhodes Island, Greece, October 2008.

[9] S. H. Han and J. H. Lee, "An overview of peak-to-average power ratio reduction techniques for multicarrier transmission," *IEEE Wireless Communications*, vol. 12, no. 2, pp. 56–65, 2005.

[10] T. Jiang and Y. Wu, "An overview: peak-to-average power ratio reduction techniques for OFDM signals," *IEEE Transactions on Broadcasting*, vol. 54, no. 2, pp. 257–268, 2008.

[11] J. Tellado, *Peak to average power reduction for multicarrier modulation*, Ph.D. dissertation, Stanford University, Stanford, Calif, USA, 2000.

[12] B. S. Krongold and D. L. Jones, "An active-set approach for OFDM PAR reduction via tone reservation," *IEEE Transactions on Signal Processing*, vol. 52, no. 2, pp. 495–509, 2004.

[13] S. Janaaththanan, C. Kasparis, and B. G. Evans, "A gradient based algorithm for PAPR reduction of OFDM using tone reservation technique," in *Proceedings of the 67th IEEE Vehicular Technology Conference (VTC '08)*, pp. 2977–2980, Marina Bay, Singapore, May 2008.

[14] R. W. Bäuml, R. F. H. Fischer, and J. B. Huber, "Reducing the peak-to-average power ratio of multicarrier modulation by selected mapping," *Electronics Letters*, vol. 32, no. 22, pp. 2056–2057, 1996.

[15] M. Breiling, S. H. Mller-Weinfurtner, and J. B. Huber, "SML peak-power reduction without explicit side information," *IEEE Communications Letters*, vol. 5, no. 6, pp. 239–241, 2001.

[16] B. S. Krongold and D. L. Jones, "PAR reduction in OFDM via active constellation extension," *IEEE Transactions on Broadcasting*, vol. 49, no. 3, pp. 258–268, 2003.

[17] ETSI EN 302 755, "Digital video broadcasting (DVB); frame structure channel coding and modulation for a second generation digital terrestrial television broadcasting system (DVB-T2)," April 2008.

[18] D. C. Chu, "Polyphase codes with good periodic correlation properties," *IEEE Transactions on Information Theory*, vol. 18, no. 4, pp. 531–532, 1972.

[19] A. J. Viterbi, *CDMA Principles of Spread Spectrum Communications*, Addison-Wesley Wireless Communications Series, Addison-Wesley, Reading, Mass, USA, 2nd edition, 1995.

[20] ETSI TR 102 377, "Digital video broadcasting (DVB); DVB-H implementation guidelines," v1.2.1, November 2005.

[21] M. Papaleo, R. Firrincieli, S. Cioni, et al., "Link layer FEC in DVB-RCS: performance evaluation in nLoS conditions," in *Proceedings of the 67th IEEE Vehicular Technology Conference (VTC '08)*, pp. 2972–2976, Marina Bay, Singapore, May 2008.

[22] M. Papaleo, R. Firrincieli, G. E. Corazza, and A. Vanelli-Coralli, "On the application of MPE-FEC to mobile DVB-S2: performance evaluation in deep fading conditions," in *Proceedings of the International Workshop on Satellite and Space Communication (IWSSC '07)*, pp. 223–227, Salzburg, Austria, September 2007.

[23] F. Pérez-Fontán, M. Vázquez-Castro, C. E. Cabado, J. P. García, and E. Kubista, "Statistical modeling of the LMS channel," *IEEE Transactions on Vehicular Technology*, vol. 50, no. 6, pp. 1549–1567, 2001.

[24] ETSI TM-SSP252-Revision 6 (2007-05), "Digital video broadcasting (DVB); DVB-SH implementation guidelines".